2010

Mineralogical and Chemical Characteristics of Some Natural Jarosites

George A. Desborough
U.S. Geological Survey, Box 25046, M.S. 973, Denver, CO 80225-0046, USA

Kathleen S. Smith
U.S. Geological Survey, Box 25046, M.S. 964D, Denver, CO 80225-0046 , USA

Heather A. Lowers
U.S. Geological Survey, Box 25046, M.S. 973, Denver, CO 80225-0046, USA

Gregg A. Swayze
U.S. Geological Survey, Box 25046, M.S. 964D, Denver, CO 80225-0046 , USA

Jane M. Hammarstrom
U.S. Geological Survey, 12201 Sunrise Valley Drive Mail Stop 954, Reston, VA 20192, USA

See next page for additional authors

Available online at www.sciencedirect.com
ScienceDirect
Geochimica et Cosmochimica Acta 74 (2010) 1041–1056
Geochimica et Cosmochimica Acta
www.elsevier.com/locate/gca

Mineralogical and chemical characteristics of some natural jarosites

George A. Desborough [a], Kathleen S. Smith [b,*], Heather A. Lowers [a], Gregg A. Swayze [b], Jane M. Hammarstrom [c], Sharon F. Diehl [b], Reinhard W. Leinz [b], Rhonda L. Driscoll [a]

[a] U.S. Geological Survey, Box 25046, M.S. 973, Denver, CO 80225-0046, USA
[b] U.S. Geological Survey, Box 25046, M.S. 964D, Denver, CO 80225-0046 , USA
[c] U.S. Geological Survey, 12201 Sunrise Valley Drive Mail Stop 954, Reston, VA 20192, USA

Received 5 November 2008; accepted in revised form 5 November 2009; available online 10 November 2009

Abstract

This paper presents a detailed study of the mineralogical, microscopic, thermal, and spectral characteristics of jarosite and natrojarosite minerals. Systematic mineralogic and chemical examination of a suite of 32 natural stoichiometric jarosite and natrojarosite samples from diverse supergene and hydrothermal environments indicates that there is only limited solid solution between Na and K at low temperatures, which suggests the presence of a solvus in the jarosite-natrojarosite system at temperatures below about 140 °C. The samples examined in this study consist of either end members or coexisting end-member pairs of jarosite and natrojarosite. Quantitative electron-probe microanalysis data for several natural hydrothermal samples show only end-member compositions for individual grains or zones, and no detectable alkali-site deficiencies, which indicates that there is no hydronium substitution within the analytical uncertainty of the method. In addition, there is no evidence of Fe deficiencies in the natural hydrothermal samples. Hydronium-bearing jarosite was detected in only one relatively young supergene sample suggesting that terrestrial hydronium-bearing jarosites generally are unstable over geologic timescales.

Unit-cell parameters of the 20 natural stoichiometric jarosites and 12 natural stoichiometric natrojarosites examined in this study have distinct and narrow ranges in the *a*- and *c*-cell dimensions. There is no overlap of these parameters at the 1σ level for the two end-member compositions. Several hydrothermal samples consist of fine-scale (2–10 μm) intimate intergrowths of jarosite and natrojarosite, which could have resulted from solid-state diffusion segregation or growth zoning due to variations in the Na/K activity ratio of hydrothermal solutions.
Published by Elsevier Ltd.

1. INTRODUCTION

Jarosite-group minerals are members of the jarosite subgroup (where $B = Fe^{+3} > Al^{+3}$), within the alunite supergroup $[AB_3(XO_4)_2(OH)_6]$, and $A = Na^+$, K^+, Ag^+, Rb^+, H_3O^+, NH_4^+, Pb^{+2}; and $B = Fe^{+3}$, Al^{+3}, Cr^{+3}; and X = S > As or P (Jambor, 1999; Dutrizac and Jambor, 2000). They are trigonal (hexagonal) in space group R-3 m. There is a wide variety of jarosite-group minerals with variable chemical properties. The chemical formula for end-member jarosite is $KFe_3(SO_4)_2(OH)_6$; it has unit-cell parameters of $a \cong 7.3$ Å, $c \cong 17.2$ Å. Natrojarosite is the sodium analog of jarosite and has $a \cong 7.33$ Å, $c \cong 16.7$ Å, and a chemical formula of $NaFe_3(SO_4)_2(OH)_6$. There can be substitution of hydronium ion (H_3O^+) for K^+ or Na^+ in the A site of jarosite and natrojarosite. Stoffregen et al. (2000) present an overview of jarosite-group minerals, including crystallography and cell dimensions of end members.

* Corresponding author. Tel.: +1 303 236 5788.
E-mail address: ksmith@usgs.gov (K.S. Smith).

0016-7037/$ - see front matter Published by Elsevier Ltd.
doi:10.1016/j.gca.2009.11.006

This paper discusses the chemical composition and unit-cell parameters of several natural stoichiometric jarosites and natrojarosites. This study evolved from our work with hard-rock metal-mine-waste characterization in which our chemical and mineralogical studies of acid-generating waste material led to examination of jarosite-group minerals as potential sources of acid generation. As a part of this work, we were interested in determining if solid solution between Na, K, and H_3O has an effect on the stability of natural jarosite-group minerals. In particular, we were interested in determining if there is significant hydronium substitution for K and Na in the monovalent cation site of natural jarosite minerals from mine-waste material. Our approach to address these questions included accumulating 23 natural jarosite-mineral samples from diverse low-temperature and hydrothermal environments and systematically examining their mineralogical and chemical properties using X-ray diffraction, quantitative electron-probe microanalysis, static and dynamic heating studies, and spectral measurements.

1.1. Jarosite as an acid generator in mining wastes

Acid can be generated by mining wastes due to the oxidation of sulfide minerals, the dissolution of soluble sulfate salts (e.g., Cravotta, 1994; Jambor et al., 2000), and the dissolution of less-soluble sulfate minerals, such as jarosite-group minerals (Alpers et al., 1994). Hydronium-bearing jarosite, in particular, is thought to contribute to acid generation in mining wastes (Lapakko and Berndt, 2003; Gasharova et al., 2005). However, the oxidation of iron-sulfide minerals, such as pyrite [FeS_2], generally is responsible for most of the acid generated by mining wastes.

Jarosite-group minerals commonly form as secondary phases in the weathered zone of sulfide-bearing mineral deposits and sulfide-bearing sediments; hence, they commonly are associated with acid-generating mining wastes and acid–sulfate soils. Jarosite minerals also are produced as a by-product of the metal processing industry. Jarosite minerals precipitate from sulfate-rich waters in the pH range of 1–3 (Alpers et al., 1989). Because of their association with acidic conditions, jarosite minerals can be used as a proxy in remote-sensing studies to locate areas of high acidity (Swayze et al., 2000).

The role of jarosite-group minerals as potential sources of acid has been a controversial subject. Welch et al. (2008), and references therein report that jarosite can be a major source of acidity in some Australian coastal soils. Jarosite can generate acid by the following reaction:

$$KFe_3(SO_4)_2(OH)_6 \rightarrow 3FeO(OH) + K^+ + 2SO_4^{2-} + 3H^+$$

Smith et al. (2006) demonstrated that jarosite dissolution is incongruent, with selective dissolution of K and SO_4. This complicates determination of jarosite solubility constants (K_{sp}); published K_{sp} values for jarosite range over several orders of magnitude. A further complication is that natural jarosite-group minerals cannot be isolated in low-temperature, supergene environments due to their small size (generally <2 μm, often <0.5 μm). Hence, in natural systems it is difficult to determine jarosite-mineral contributions to acid generation. For example, even minor amounts of soluble sulfate salts can contribute to acidic conditions upon wetting (Nordstrom and Alpers, 1999).

Field and laboratory studies of 130 metal-mine-waste piles in the Rocky Mountain region by the U.S. Geological Survey (USGS) showed that the presence of jarosite minerals in wastes was the best indicator of acid-generation potential (Desborough et al., 1999). For the study area of the Animas River headwaters, Colorado, 70 samples with X-ray diffraction (XRD)-detectable jarosite-group minerals produced a final leachate median pH value of 3.5 with a range of 2.6–6.6. In contrast, for 41 samples from the same area without XRD-detectable jarosite, the median leachate pH value was 4.7 with a range of 2.8–7.7. For the Boulder River headwaters study area in Montana, 15 samples with XRD-detectable jarosite had a median leachate pH value of 3.7 with a range of 2.7–5.9; for four samples without detectable jarosite, the median pH value was 5.1 with a range of 3.2–6.8. These laboratory leaching results indicate that fine-grained jarosite originating from surficial weathering or oxidation of iron sulfide(s) may be a significant source of acid generation.

Alpers et al. (1989) point out that both chemical composition and particle size are recognized as important factors in jarosite solubility. To address the importance of particle size, Desborough et al. (2006) used several different size fractions of one high-purity end-member K-jarosite to demonstrate significant acid generation in deionized water (jarosite:water = 1:100) in an eight-day and a 27.5-month exposure. These experiments demonstrated the strong effects of different size fractions on jarosite solubility. In that same study they exposed four synthetic hydronium-bearing jarosites and one synthetic hydronium-free jarosite to deionized water (jarosite:water = 1:100) for eight-day and 27.5-month periods, respectively. They found that the most hydronium-rich jarosite (largest *a*-cell dimension) generated the greatest acidity, whereas the hydronium-free jarosite (smallest *a*-cell dimension) generated the least acidity. In addition, they found that the common practice of heating synthetic non-stoichiometric jarosites or hydronium-bearing jarosites above about 100 °C during "drying" changes their structural nature by driving off water molecules in vacant alkali or protonated hydroxyl sites, or both, when these sites are occupied by water. This result would alter their cell dimensions, chemical composition, and stability (or solubility), which affects study results if the purpose of synthesis was to mimic natural jarosites formed in supergene environments (such as mine-waste piles).

In addition to mining wastes, there are large quantities of K-rich or Na-rich synthetic jarosites formed as a by-product of hydrometallurgical recovery of zinc from ores. These by-products are recognized as acid-producing wastes (Dutrizac and Kaiman, 1976; Dutrizac and Jambor, 2000). Because these synthetic by-product jarosites are unstable, they require additives to stabilize the waste to prevent acid generation (Seyer et al., 2001).

1.2. Characteristics of supergene jarosite minerals

Low-temperature, supergene jarosite minerals form in a variety of environments. It is common, but not necessary, for low-temperature jarosites to form as a result of pyrite oxidation. The environment of formation is important in controlling conditions of jarosite crystallization, which affects stability and solubility. Low-temperature jarosites tend to be very-fine-grained, and jarosites in mining waste are concentrated in the <325 mesh (<45 μm) screen fraction, but are intimately admixed with associated minerals such as quartz and iron oxides. Scanning electron microscope (SEM) studies show that many of the jarosite grains in mining wastes are smaller than 0.5 μm (Desborough et al., 2006). This small grain size prohibits separation of jarosite for chemical analysis and makes the grains too small for electron microbeam analysis.

Jarosite-group minerals have been identified at a number of mining districts. For example, Butler et al. (1920) recognized jarosite as a low-temperature oxidation product of sulfides in the Tintic district of Utah. Alpers and Brimhall (1989) described jarosite in leached cappings of a porphyry copper deposit in northern Chile. Stable isotopes of supergene jarosite from Paradise Peak and the Pioche district in Nevada, and the Apex mine in Utah studied by Rye and Alpers (1997) revealed characteristics of low-temperature environments. Jamieson et al. (2005) described jarosite-group minerals in the form of stalactites and in fine-grained mud forming underground in the Richmond mine at Iron Mountain, California where the water had a pH of about 2.1.

Jarosite minerals also have been identified in a variety of other low-temperature environments. For example, Van Breemen (1982, p. 98), reports "The pale yellow mottles [of jarosite] are so characteristic [of acidic soils] that they are used, together with pH, as a diagnostic criterion for classifying acid–sulfate soils" (USDA, 1975). Wagner et al. (1982) found that jarosite may persist in Maryland soils long after sulfide oxidation has ceased. Polyak and Provencio (2001, Table 1) listed jarosite as a "primary speleogenetic by-product" in the Carlsbad caves of southeastern New Mexico, where the sulfate components originated from oxidation of H_2S to form H_2SO_4. Rodriguez et al. (2005) reported the presence of jarosite in plant tissues in a perennial grass (*Imperata cylindrical*) growing along the banks of the Tinto River in the Iberian Pyritic Belt in Spain. Recently, jarosite has been identified as one of the hydrated minerals discovered by the Opportunity Rover at Eagle Crater on Mars (Klingelhöfer et al., 2004), and Milliken et al. (2008) report spectral detection of hydronium-bearing jarosite in deposits on the plains surrounding the Valles Marineris canyon system on Mars.

Microbial processes can influence jarosite formation. Ivarson (1973) was among the first to demonstrate the influence of *Acidithiobacillus ferrooxidans* on jarosite formation. Ivarson et al. (1982) and Ross et al. (1982) later demonstrated "room temperature" formation of jarosite, natrojarosite, ammoniojarosite, and hydronium jarosite, which occurred over periods of several days to several weeks using *A. ferrooxidans*. Ross et al. (1982, Fig. 12) reported coexisting natural jarosite and natrojarosite in six soil samples from five Canadian provinces and Ellef Ringes Island (arctic soil).

1.3. Characteristics of hydrothermal jarosite minerals

Hydrothermal jarosites typically form in highly oxidized, epithermal, near-surface environments of low pH. Hydrothermal jarosites are formed at high temperature (typically 100–300 °C), and are well-crystallized and larger in size than supergene jarosites. Steam-heated jarosites occur in ore deposits at Marysvale, Utah and the Sulfur and Gilbert mining districts in Nevada (Rye and Alpers, 1997). Lueth et al. (2005) studied stable isotopes of 24 "sour gas" hydrothermal jarosite samples from 14 mines in northern Mexico and New Mexico and reported $^{39}Ar/^{40}Ar$ dates ranging from about 0.5 to 9.4 Ma. Martinez-Frias et al. (2004) described the setting of jarosite at the type locality (El Jaroso, Spain) as a multistage hydrothermal deposit with fluid inclusion homogenization temperatures between 150 and 360 °C.

2. EXPERIMENTAL METHODS

2.1. Analytical and experimental methods

X-ray powder diffraction patterns were obtained with a Shimadzu XRD-6000 diffractometer operated at 40 kV and 30 mA at a scan speed of 2° 2θ/min. using Cu Kα radiation ($\lambda = 1.54056$ Å). Diffractometer patterns of all jarosites were first obtained to determine the number of jarosite phases present (i.e., purity) and the associated minerals. Calibration was obtained using Linde C, 1.0 μm alumina powder (Union Carbide Corp.) as an internal standard at a concentration of 10 weight percent in each sample; PDF No. 46-1212 of the ICDD Powder Diffraction Files (2002 edition) was used for the diffraction lines and cell parameters of the alumina. Cell parameters of the jarosite samples were calculated by least squares refinement methods with the JADE (v.7.0) software of Materials Data Inc., Livermore, California.

Chemical compositions were obtained for nine polished thin sections of natural samples using a JEOL JXA-8900 fully automated five spectrometer electron microprobe. Well-characterized silicate and oxide standards were used for calibration. Operating conditions were 15 kV, 10 nA (cup), and an electron beam defocused to 5-μm diameter to reduce Na and K migration. The excitation volume existing when the 5-μm diameter electron beam enters the sample is about 8 μm^3 under the analytical conditions used. Analytical uncertainty for major and minor elements is about ±2% (1σ) and about ±3% for trace elements, based on counting statistics. For the electron microprobe data, we assumed that there was one mole of combined $K + Na + H_3O$ for each two sulfur atoms. For two samples of natural jarosites, K and Na concentrations were measured by inductively-coupled plasma mass spectrometry (ICP-MS) on solutions obtained by a four-acid digestion (Briggs and Meier, 2002).

Static heating studies were performed in a thermocouple-controlled Thermolyne furnace using about 0.2–0.5 g of jarosite mixed with 10 weight percent alumina in 10 ml mullite crucibles. Weight losses were measured and all run products were examined by X-ray diffraction analysis in order to identify phases and measure cell parameters of jarosite-group minerals.

Mass loss as a function of dynamic (continuous) heating was studied by thermogravimetric analysis (TGA) with simultaneous evolved gas analysis. Two jarosite samples (Pena Blanca II and 81196u) and one natrojarosite sample (Cyprus) were run in a Mettler TGA/SDTA851e thermal analyzer coupled to a Balzers quadrupole mass spectrometer (QMS). Approximately 10 mg of jarosite was placed in a pre-weighed, 70-μl aluminum-oxide crucible. Samples were heated from 25 to 1100 °C at a rate of 10 °C/min. in an atmosphere of flowing argon (75 ml/min); appropriate mass numbers for water, CO_2, SO_2, O_2, and N_2 as probable parent molecules for any evolved gas species were monitored during the runs. Sample mass, sample purity, particle size, heating rate and furnace atmosphere can all affect reaction temperatures (Bish and Duffy, 1990).

Transmission spectra of jarosite samples were obtained from pellets composed of 0.7 mg of finely-ground jarosite sample mixed with 0.3 g of KBr. Measurements were made using a Nicolet Magna Fourier Transform Infra-Red (FTIR) interferometer spectrometer. Spectra were measured over a range of about 2–25 μm at 4 cm^{-1} spectral resolution. The KBr was dehydrated at 110 °C prior to mixing and then the mixture was compressed at 10 metric tons for 5 min under a vacuum. R. Stoffregen provided a synthesized 250 °C intermediate-composition jarosite for spectral measurement (see Stoffregen, 1993 for synthesis information).

2.2. Sample descriptions

The samples used for this study are from diverse environments of formation and are listed in Table 1. The jarosite sample from the Gunma Iron Mine in Japan was precipitated in a spring (22 °C) with a pH of 2.8 (Akai et al., 1997). A natrojarosite from South Mineral Creek, near Silverton, Colorado, was found on a log in an iron bog with a pH of 3.3–3.4 and occurs as 1–15 μm crystals associated with opaline silica and underlain by schwertmannite. The three jarosite/natrojarosite pairs from Chuquicamata, Chile are of supergene origin from the oxidized zone of a porphyry copper deposit (Rye and Alpers, 1997). The jarosite samples from the Pena Blanca mine, Mexico occur as coarse hydrothermal crystals that formed at about 180 °C (P.C. Goodell, personal communication cited in Lueth et al., 2005); $^{40}Ar/^{39}Ar$ dating shows that the jarosite formed at around 9.42 Ma ± 0.11 Ma (Lueth et al., 2005). Three pairs of jarosite/natrojarosite from the Copiapo mine in the Franklin mining district in New Mexico are hydrothermal, and $^{40}Ar/^{39}Ar$ ages range from about 3 to 5 Ma (Lueth et al., 2005). The four Jaroso samples of hydrothermal origin are from the jarosite type locality in Spain.

3. STOICHIOMETRIC JAROSITE MINERALS

3.1. Unit-cell parameters

Changes in unit-cell parameters can be diagnostic of element substitutions or vacancies within the unit cell, which can lead to decreased stability of a mineral phase. Natrojarosite has a much smaller unit-cell volume than does jarosite due to the smaller diameter of the sodium ion. The *a*- and *c*-cell dimensions for the natural stoichiometric jarosite and natrojarosite samples examined in this study are shown in Fig. 1, and cell parameters are given in Table 1. Summary statistics for these two groups are reported in Table 2. Four hydrothermal samples and five supergene samples consisted of pairs of both end-member jarosite and end-member natrojarosite; these nine pairs of jarosite and natrojarosite are listed together in Table 1 and their unit-cell dimensions are included in Fig. 1. Fig. 2 is an illustration of a segment of X-ray diffractometer scans showing how jarosite and natrojarosite end members differ in the position of the 006 (hkl) reflection; results for a mixture of jarosite and natrojarosite are also shown. For the 23 stoichiometric hydrothermal and supergene samples examined in this study, jarosite and natrojarosite cell dimensions, respectively, occur in two distinct groups that do not overlap (Fig.1 and Table 2). If there were significant solid solution between jarosite and natrojarosite, cell dimensions intermediate between jarosite and natrojarosite end-members would be observed (Stoffregen et al., 2000, Fig. 13).

Cell dimensions determined in this study for natural samples are in reasonable agreement with published values. Kato and Miúra (1977) obtained $a = 7.304 \pm 0.002$, $c = 17.268 \pm 0.005$ for jarosite from Pioche, Nevada, and Warshaw (1956) reported cell parameters for jarosite ($a = 7.29$, $c = 17.22$) in coal underclays in Pennsylvania. Mitchell and Giannini (1958) reported $a = 7.34$, $c = 16.72$ in sedimentary rocks of southern Montana. Other cell parameters for jarosites listed in literature include seven from Alpers et al. (1989), which are laboratory precipitates from filtered, natural acidic water from Iron Mountain, California. In addition, Alpers et al. (1992) listed cell parameters of three jarosite samples from Australian lakes, but these have significant Al substituted for Fe.

3.2. Chemical composition

Electron-probe microanalysis (EPMA) was performed on polished thin sections of eight solid samples and one polished thin section grain mount with 100- to 200-μm grains (sample PB-II). Results are given for the nine samples in Table 3, along with results obtained by ICP-MS analyses for three samples. It must be noted that the samples used for EPMA are not necessarily identical to those used for X-ray diffraction (XRD) studies because samples are inhomogeneous with regard to proportions of jarosite and natrojarosite. Specifically, EPMA may reveal the presence of small amounts of jarosite or natrojarosite that were not detected by XRD analysis. It is also important to note that the size of chemical domains in some of these samples is too small to resolve by EPMA with a 5-μm diameter

Table 1
Locations, sources, associated minerals, and cell parameters of natural stoichiometric jarosites and natrojarosites used in this study.

Sample Name	Location	Source	Associated minerals	Classification	*a* (Å)	*c* (Å)	Lines used	Volume (Å^3)
Supergene or secondary								
Cassington	Oxford, England	1	Quartz, kaolinite, gypsum	K	7.307 (8)	17.16 (2)	22	793.45
				Na	7.319 (5)	16.75 (2)	20	777.19
Chuquicamata (dark brown)	Chile	2	None	Na	7.325 (7)	16.60 (2)	25	771.2
				K	7.305 (4)	17.20 (1)	25	794.93
Chuquicamata (tan)	Chile	2	None	K	7.307 (4)	17.22 (1)	22	796.19
				Na	7.327 (7)	16.59 (2)	23	771.25
Chuquicamata (yellow)	Chile	2	None	Na	7.320 (8)	16.71 (2)	22	775.46
				K	7.306 (5)	17.19 (2)	20	794.7
Cyprus (Skouriatissa)	Cyprus, Greece	1	None	Na	7.317 (2)	16.58 (4)	27	768.47
Gunma Iron Mine	Japan	3	None	K	7.308 (2)	17.22 (6)	25	796.63
Silver Cliff Mining District	Custer County, CO	3	Calcite, orthoclase, quartz	K	7.308 (7)	17.17 (2)	25	794.12
				Na	7.320 (8)	16.69 (2)	24	774.34
South Mineral Creek	Silverton, CO	3	Schwertmannite, opal	Na	7.330 (2)	16.69 (7)	10	775.05
81196u	(proprietary)	4	Quartz, gypsum	K	7.307 (5)	17.22 (1)	20	795.98
Hydrothermal or hypogene								
Apex Mine	Dripping Springs Mtns., AZ	5	Goethite	K	7.310 (7)	17.20 (2)	19	796.05
Centennial Eureka Mine	Juab County, UT	1	Quartz, goethite	Na	7.326 (4)	16.615 (7)	24	772.12
Copiapo Mine	Franklin mining district, NM	2	None	Na	7.330 (1)	16.60 (1)	17	773.77
				K	7.311 (7)	17.22 (1)	14	797.25
CJ96-98 (Copiapo N.L. 1 Mine)	Franklin mining district, NM	2	Quartz	Na	7.322 (9)	16.66 (2)	22	773.36
				K	7.304 (6)	17.18 (1)	23	793.97
CJ96-124 (Copiapo N.L. 5 Mine)	Franklin mining district, NM	2	Quartz	K	7.306 (8)	17.17 (2)	19	793.75
				Na	7.320 (9)	16.65 (1)	21	772.24
FeBL (Iron Blossom Mine)	Tintic, UT	3	Quartz	K	7.302 (4)	17.208 (9)	23	794.49
Jaroso-I (Barranco del Jaroso)	Sierra Almagera, Spain	1	None	K	7.290 (4)	17.202 (7)	23	794.84
Jaroso-II (Barranco)	Almeria, Spain	6	Goethite, amorphous Fe-oxide	K	7.305 (9)	17.220 (7)	22	795.71
Jaroso-III (Barranco)	Almeria, Spain	1	Amorphous Fe-oxide	K	7.308 (2)	17.234 (3)	12	797.23
Jaroso-IV (Barranco)	Almeria, Spain	1	Hematite	K	7.299 (4)	17.172 (2)	13	792.72
LTNV (Lone Tree Mine)	Humboldt County, NV	1	Dufretite	K	7.302 (7)	17.218 (1)	14	794.95
Najar-II (Laurium)	Attica Peninsula, Greece	1	Scorodite	K	7.308 (3)	17.233 (4)	18	797
				Na	7.320 (1)	16.715 (3)	21	776.38
PB97-01 (Pena Blanca Mine)	Mexico	2	None	K	7.299 (4)	17.234 (6)	25	795.08
PB-II (Pena Blanca Mine)	Mexico	7	Kaolinite	K	7.294 (3)	17.236 (3)	15	794.16

Sources: (1) Excalibur Mineral Corp., Peekskill, NY; (2) Robert Rye, USGS (and V. Lueth, NM BGMR); (3) USGS; (4) Kim Lapakko, MN DNR; (5) Adams Minerals, Grand Junction, CO; (6) Carel Meijboom, Zutphen, Netherlands; and (7) Prof. Goodell, Univ. Texas (El Paso).
Classification: Na, natrojarosite, K, jarosite.
Numbers in parentheses are least-square standard errors.

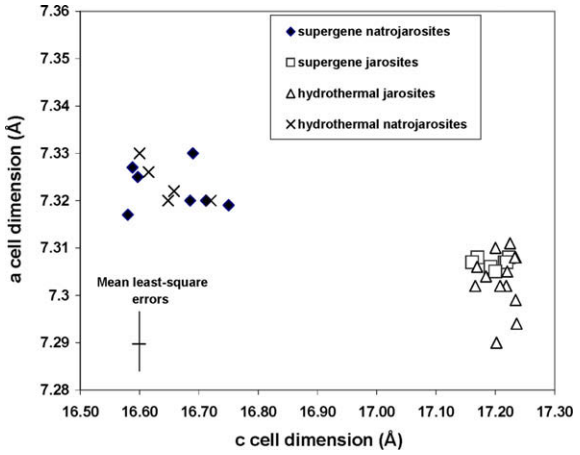

Fig. 1. Cell dimensions of 20 natural stoichiometric jarosite and 12 stoichiometric natrojarosite samples as measured in this study. Data include nine coexisting pairs of end-member jarosite and natrojarosite.

Table 2
Statistical summary for unit-cell parameters of 20 natural stoichiometric jarosites and 12 natural stoichiometric natrojarosites.

	a-Cell dimension (Å)	*c*-Cell dimension (Å)	Volume (Å^3)
Jarosites			
Mean	7.304	17.206	795.16
Range	7.29–7.31	17.16–17.23	–
Std. Error	0.001	0.006	0.3
Std. Dev.	0.005	0.02	1.3
95% Conf. level for mean	0.002	0.01	0.6
Natrojarosites			
Mean	7.323	16.653	773.3
Range	7.32–7.33	16.58–16.75	–
Std. Error	0.001	0.017	0.8
Std. Dev.	0.005	0.06	2.5
95% Conf. level for mean	0.003	0.04	1.7

Ten weight percent alumina (Al_2O_3) was used as an internal standard for each sample.

electron beam. Papike et al. (2006, 2007) reveal that even a small electron beam could not resolve sub-micrometer intergrowths of jarosite and natrojarosite in samples from Goldfield, Nevada and from more than a dozen other localities worldwide.

Data in Table 3 show that Jaroso-I, from the type locality, is a homogeneous end-member jarosite with only a small amount of aluminum substituted for iron; backscattered electron (BSE) images indicate only one phase is present. The three other samples of Jaroso are more complex and have compositional variations due to the presence of small amounts of sub-micrometer domains of natrojarosite that are too small to be resolved by EPMA. Jaroso-II BSE images show zoning, which corresponds to variations in both Na and Pb (Table 3 and Fig. 3a). Lead concentrations reach as much as 5 mol%, but Pb was below the detection limit for 13 of the 32 analyses. Although the mean K content is 89 mol% for 23 of the 32 analyses, the mean K content for 9 analyses is 97 mol% with a standard deviation of 4 mol%. Jaroso-III images for Na show a zoned distribution with distinct variations in Na concentrations (Fig. 3b), which range up to 60 mol%. Although the mean K content is only 84 mol% for 36 analyses (Table 3), for 16 of the 36 analyses the mean K content is 96 mol% ($\sigma = 4$ mol%) and Na is 4 mol% ($\sigma = 3$ mol%). Jaroso-IV BSE images show fine-scale growth zoning (Fig. 3c) that appears to be related to variations in Pb and Na concentrations. Although K is dominant (Table 3), both Pb and Na are significant components of the jarosite(s); K ranges up to 94 mol%, Na ranges up to 52 mol%, and Pb ranges up to 29 mol%. The individual segregations of jarosite(s) are so small that EPMA does not resolve end-member jarosite, although XRD data indicate that end-member jarosite is the dominant phase (Table 1).

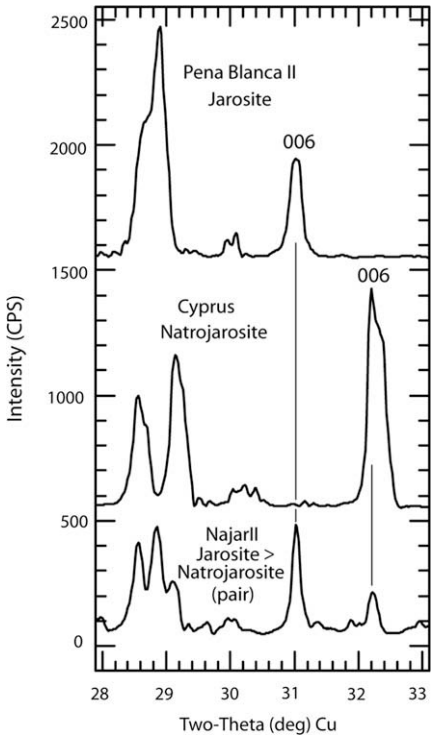

Fig. 2. X-ray diffractograms showing the distinct separations of the 006 (hkl) reflections of end-member jarosite and end-member natrojarosite, and mixtures of both end members.

The Pena Blanca II sample from Mexico (PB-II) is end-member jarosite, like Jaroso-I, except for the small amounts of Al substituting for Fe in both (Table 3). BSE images show good homogeneity. Sample FeBL from the Iron Blossom mine at Tintic, Utah consists of intergrowths of rectangular segregations resolved in BSE images (Fig. 3d). The nature of the distribution of different phases shown by BSE images is not consistent with a distribution of phases due to primary zoning. Rather it seems to be due to unmixing by solid-state diffusion redistribution of elements during subsolidus cooling. The X-ray diffraction traces show only major jarosite and minor quartz (Table 1). However, the EPMA data show major K, minor Sr and Na, along with

Table 3
Molar compositions of jarosites and natrojarosites determined by electron-probe microanalysis (EPMA) and inductively-coupled plasma mass spectroscopy (ICP-MS).

Sample name	*n*		A						B		X				
			Na	K	Pb	Ca	Sr	Ba	Fe	Al	S	As	P	ΣA	ΣB
FeBL	42	Mean	0.05	0.73	bdl	bdl	0.14	0.05	2.83	0.06	1.68	0.32	bdl	0.97	2.89
		1σ	0.07	0.12	–	–	0.08	0.04	0.07	0.04	0.15	0.15	–	–	–
Jaroso-I	34	Mean	0.02	1.01	bdl	bdl	bdl	bdl	2.99	0.11	2.00	bdl	bdl	1.03	3.10
		1σ	0.02	0.03	–	–	–	–	0.11	0.10	0.00	–	–	–	–
Jaroso-II	32	Mean	0.10	0.90	bdl	bdl	bdl	bdl	2.98	0.09	2.00	bdl	bdl	1.00	3.07
		1σ	0.13	0.14	–	–	–	–	0.10	0.11	0.00	–	–	–	–
Jaroso-III	36	Mean	0.17	0.84	bdl	bdl	bdl	bdl	2.97	0.04	2.00	bdl	bdl	1.01	3.01
		1σ	0.17	0.17	–	–	–	–	0.09	0.04	0.00	–	–	–	–
Jaroso-IV	26	Mean	0.12	0.72	0.16	bdl	bdl	bdl	2.80	0.14	2.00	bdl	bdl	1.00	2.94
		1σ	0.15	0.13	0.07	–	–	–	0.09	0.07	0.00	–	–	–	–
LTNV	14	Mean	0.06	0.93	bdl	bdl	bdl	bdl	2.79	0.15	1.97	0.03	bdl	0.99	2.94
		1σ	0.06	0.07	–	–	–	–	0.12	0.12	0.02	0.01	–	–	–
	8	Mean	0.90	0.11	bdl	bdl	bdl	bdl	2.97	0.02	2.00	bdl	bdl	1.01	2.99
		1σ	0.10	0.09	–	–	–	–	0.08	0.02	0.01	–	–	–	–
Najar-II	19	Mean	0.02	0.98	bdl	bdl	bdl	bdl	2.99	bdl	1.91	0.09	bdl	1.00	2.99
		1σ	0.02	0.02	–	–	–	–	0.04	–	0.04	0.04	–	–	–
	27	Mean	1.01	bdl	bdl	bdl	bdl	bdl	2.98	bdl	1.97	0.03	bdl	1.01	2.98
		1σ	0.04	–	–	–	–	–	0.08	–	0.01	0.01	–	–	–
PB-II	53	Mean	bdl	0.99	bdl	bdl	bdl	bdl	2.82	0.13	2.00	bdl	bdl	0.99	2.95
		1σ	0.00	0.03	–	–	–	–	0.07	0.05	0.00	–	–	–	–
81196u	26	Mean	0.06	0.84	bdl	bdl	bdl	bdl	2.91	0.05	1.91	0.09	bdl	0.90	2.96
		1σ	0.04	0.08	–	–	–	–	0.12	0.03	0.10	0.10	–	–	–
ICP-MS analysis for Na and K only															
Cyprus	1	Mean	0.97	<0.01											
PB97-01	2	Mean	<0.01	0.97											
PB-II	4	Mean	<0.01	0.97											

Based on formula: $AB_3(XO_4)_2(OH)_6$, where A = Na, K, Pb, Ca, Sr, Ba; B = Fe^{+3}, Al; X = S, As, P. Cations were normalized to X = 2. bdl, below detection limit; *n*, number of analyses. Multiple entries for an individual sample name represent jarosite–natrojarosite near-end-member pairs.

both Ca and Ba in the A site (Table 3). In addition, substitution of As for S is significant in the X site.

Sample Najar-II from Laurium, Greece is a mixture of coarsely intergrown domains of end-member jarosite and end-member natrojarosite, along with minor scorodite [$Fe^{+3}AsO_4{\cdot}2H_2O$] (Fig. 4). The scorodite occurs as thin selvages along the margin of what might have been a solid-solution crystal of K–Na jarosite that separated into end-member jarosite and natrojarosite upon cooling. The intergrown jarosite and natrojarosite end-members do not appear to be the results of growth zoning like Fig. 3a–c, herein; they are also quite unlike the exceptional jarosite–natrojarosite growth zoning shown in Figs. 1–3 of Burger et al. (2006). The distribution of the end-members in Fig. 4 is inconsistent with growth zoning because there is an absence of lateral continuity of the end-member zones. Their boundaries are abrupt and terminal, and they end at the margins defined by scorodite. The observed textures could have formed by solid-state segregation of end members from Na–K solid-solution crystals during or after the formation of scorodite. The scorodite seems to have exsolved without significant volume change in the mass. This could be the case if equivalent fractions of H_3O and (OH) left the jarosite-natrojarosite solid solution along with the Fe and AsO_4 forming the two molecules of water in scorodite. Paktunc and Dutrizac (2004) have shown that as much as 9.9 wt.% AsO_4 can substitute for SO_4 in synthetic jarosite.

Sample 81196u is of supergene origin and consists of jarosite grains with maximum diameters on the order of a few to 10 μm; BSE images show many of these grains have hollow centers as though a precursor phase formed a nucleation center (Fig. 5). Table 3 lists the average composition for 26 analyses, but the totals indicate a deficiency in both the A and B sites; we believe this is due to the porous nature of the material and the small grain size. If the totals for the A site were correct, one could infer that the balance could be 10 mol% H_3O, 10 mol% vacancies, or a combination of both. The 4 mol% deficiency in the B site may just be due to vacancies in the trivalent site. Simultaneous measurement of Si during all of the analyses showed an average of 1 weight percent, which is taken to indicate that the electron beam was exciting a Si-bearing phase. The cell parameters indicate that the jarosite is near-end-member material, and thermal treatments at 240 and 265 °C (see below) show no change in cell dimensions, such as those observed for hydronium-bearing synthetic jarosites (Desborough et al., 2006). However, the dynamic heating experiments (see below) show a small amount of water evolved at 247 °C, from which it can be inferred that a small amount of hydronium-bearing jarosite may be present (even though it was not detected by XRD analysis).

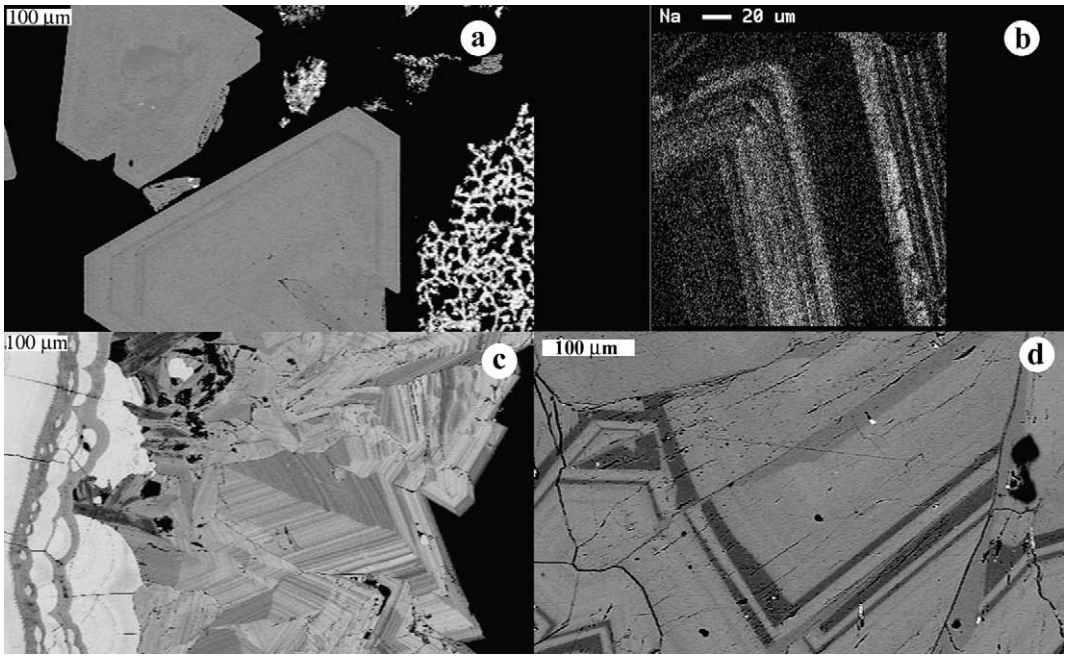

Fig. 3. Backscattered electron (BSE) images and elemental X-ray intensity maps of polished thin sections of jarosite-group samples. Scale bar is in micrometers (µm). (a) BSE image of Jaroso-II crystals showing sparse natrojarosite (darkest gray) bands in jarosite (light gray). (b) Natrojarosite bands shown by Na distribution in a Jaroso-III crystal. (c) BSE image showing complex fine-scale chemical zoning in Jaroso-IV due to variations in K, Na, and Pb. (d) BSE image showing linear features due to complex chemical variations that include significant As substitution for S in sample FeBL.

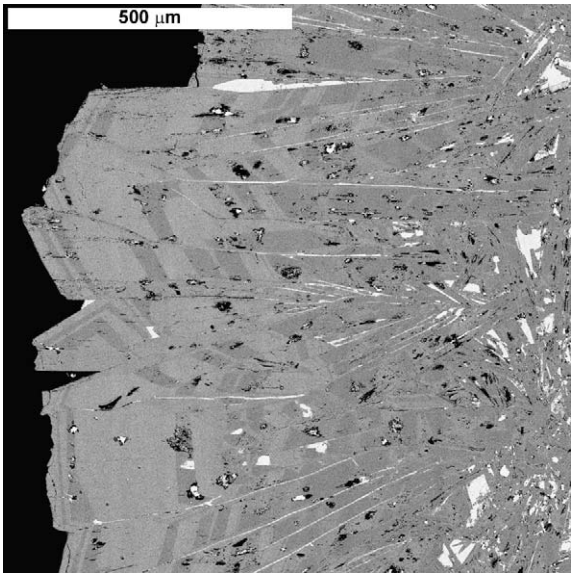

Fig. 4. BSE image of Najar-II showing scorodite selvages (white) on what we infer to be the margins of former K–Na solid-solution crystals that have subsequently become end-member jarosite (light gray) and natrojarosite (darker gray) during cooling.

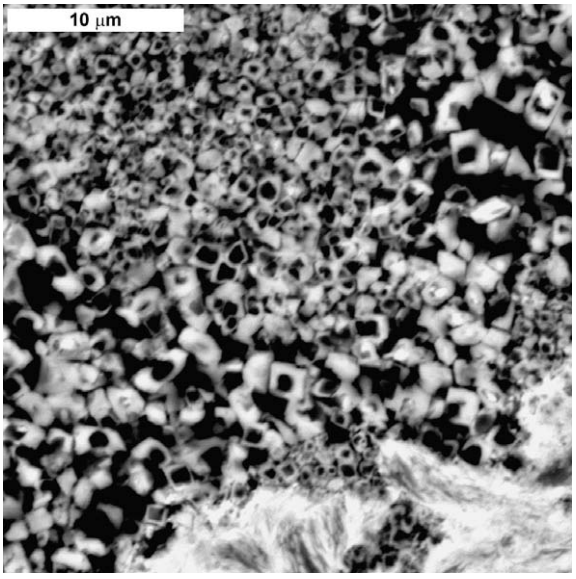

Fig. 5. High-magnification BSE image of supergene sample 81196u showing hollow cores and the highly porous nature of jarosite in crystals smaller than 5 µm.

3.3. Static heating experiments

About 0.2 g of natural samples, including five of end-member jarosite, one of natrojarosite (Cyprus, Table 1), and three with both major jarosite and major natrojarosite, were heated in 10-ml alumina crucibles at 265 °C for 24–48 h in air. These samples also contained 10 weight percent alumina as an internal standard. The five jarosite samples and the natrojarosite showed no changes in cell parameters after heating at 265 °C. However, the three samples that contained both jarosite and natrojarosite reacted to such

an extent that cell refinement was no longer satisfactory on the basis of the number of (009) hkl peaks on the diffractogram (more than two jarosite phases were present). The five jarosites and one natrojarosite samples that had been heated at 265 °C were heated again at 280 °C for 48 h; these samples remained unchanged from their unheated state. Likewise, no other changes were observed in any of the samples, including the mixtures, by further heating at 265 or 280 °C.

Seven natural samples that were heated at 380 °C for 48 h in air had no jarosite remaining. These natural samples consisted of one natrojarosite (97 mol% Na), one mixture of jarosite plus natrojarosite, and five near end-member jarosites. Except for one near-end-member jarosite (which had less yavapaiite [$KFe(SO_4)_2$] than alumina), crystalline, potassium-bearing phases were not detected by XRD analysis of the samples heated at 380 °C.

3.4. Dynamic heating experiments

Results of the dynamic heating experiments are summarized in a series of plots (Fig. 6) showing mass loss as a function of heating (TGA curve), first derivative of the TGA curve (DTG), and the evolved gas patterns (QMS) for atomic masses 18 (H_2O) and 64 (SO_2). Sulfur is released from jarosite as SO_2 gas. Note that the mass losses occur over a temperature range. Temperatures for mass loss events are arbitrarily assigned on the basis of the peaks in the derivative curve (DTG). Some mass losses are sharp; others are broad or unresolved doublets or triplets. Broad peaks and shoulders in the DTG curves are mimicked in the QMS patterns.

Supergene natrojarosite from Cyprus released 11.3 wt.% water in a single event at about 440 °C (Fig. 6a). This mass loss is in good agreement with calculated nominal natrojarosite water content (11.2%). The TGA run product consisted of a mixture of hematite and thenardite [Na_2SO_4]. Hydrothermal jarosite from the Pena Blanca mine in Mexico lost 11.2% of its starting mass at about 460 °C (Fig. 6b). This mass loss is slightly higher than the expected water content of 10.8% for end-member jarosite. Note that SO_2 evolution overlaps dehydroxylation, thus a small fraction of the mass loss arbitrarily assigned to water is probably due to sulfur loss. The higher dehydroxylation temperature of the Pena Blanca jarosite (460 °C) relative to the Cyprus jarosite (440 °C) is consistent with its K-rich composition (Kubisz, 1971). The TGA run product consisted of a mixture of hematite and arcanite [K_2SO_4], according to XRD analysis.

Supergene jarosite 81196u produced the most complicated TGA pattern of all the samples (Fig. 6c). An XRD pattern of the starting material showed that in addition to quartz, estimated at about 14 wt.%, and jarosite (81%), the sample also contained about 6 wt.% gypsum. Mixtures of several phases complicate interpretation of TGA patterns. Total mass loss attributable to water was about 10.3 wt.%, which came off in three pulses at 117, 247, and 405 °C. Note that the 405 °C water loss is a broad peak on the DTG and QMS curves that overlaps with the beginning of SO_2 evolution. The sample released SO_2 in three

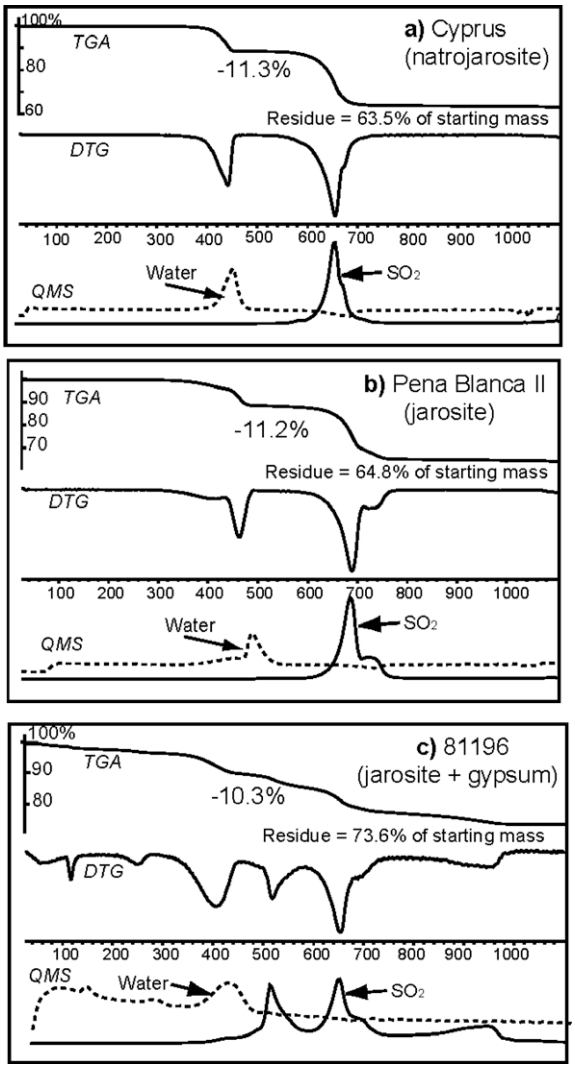

Fig. 6. Thermal analysis data for natural jarosites. Thermogravimetric pattern (TGA) shows mass loss as a function of temperature (°C; shown on the *x*-axis), mass loss attributed to water, and residue at the end of run in terms of percent of starting sample mass. DTG is the first derivative of the TGA signal, and QMS is simultaneous evolved gases determined by quadrupole mass spectrometry; the dashed line represents water (mass 18) and the solid line represents SO_2 (20 * mass 64). (a) Supergene natrojarosite from Cyprus. (b) Hydrothermal jarosite from the Pena Blanca mine, Mexico. (c) Supergene jarosite sample 81196u with minor quartz and gypsum.

stages: at about 518, 653, and 958 °C. The sample lost 26.3% of its starting mass, which is far less than would be expected for a completely reacted jarosite of any composition; pure end-member jarosite contains 10.79 wt.% water and 31.97 wt.% SO_3. The total water mass loss is consistent with the composition computed for the mixture estimated by XRD, from which 9.9 wt.% H_2O was predicted. A sample of pure gypsum analyzed with identical run parameters lost water at about 115–180 °C. We interpret the mass loss at 117 °C for jarosite 81196u as water lost from the gypsum contaminant. The mass loss at 247 °C is consistent with

water generated during destruction of a very small amount of hydronium-bearing jarosite (Alpers et al., 1989) from which liberated hydronium combines with hydroxyl (e.g., $H_3O + OH \rightarrow 2H_2O$). The 405 °C mass loss represents jarosite dehydroxylation. The mass loss contribution of SO_2 to the 405 °C event is indeterminate. Hematite, quartz, and tridymite [SiO_2] were detected by XRD of the residue; no Ca- or S-bearing phase was identified.

A number of previous studies have described the thermal behavior of different jarosites as determined by thermogravimetric analysis and (or) differential thermal analysis. Most studies however deal with synthetic minerals. Dutrizac and Jambor (2000) noted that all jarosite group minerals start to lose water at about 400 °C in dynamic heating experiments according to reactions such as:

$$KFe_3(SO_4)_2(OH)_6 \rightarrow KFe(SO_4)_2 + Fe_2O_3 + 3H_2O$$

Subsequently, $KFe(SO_4)_2$ (yavapiite) decomposes to arcanite, hematite, and SO_3:

$$2KFe(SO_4)_2 \rightarrow K_2SO_4 + Fe_2O_3 + 3SO_3$$

Alpers et al. (1989) described thermogravimetric data for jarosite precipitated in the laboratory from stored acid-mine water from Iron Mountain, CA. Their sample lost mass in three stages: (1) a single endothermic reaction at about 260 °C attributed to loss of about 4 wt.% H_3O^+, (2) a doublet at 450–480 °C corresponding to release of H_2O from hydroxyl sites, and (3) a group of three peaks at 640, 710, and 800 °C corresponding to loss of sulfur from sulfate sites. Their data and interpretations were consistent with data for other jarosites with a hydronium component (Kulp and Adler, 1950; Kubisz, 1961; Brophy and Sheridan, 1965). Kulp and Adler (1950) studied the thermal behavior of a number of natural jarosites. They described the endothermic water loss (reaction 1) at 460 °C and noted that this reaction is about 100 °C lower than the breakdown temperature observed for alunite. Their differential thermal curves for jarosites from Mexico (Santa Maria mine, Velardena and Los Lamentos, Chihauhua) are similar to the patterns we obtained for the Pena Blanca jarosite. Other natural samples in their study, including jarosite from Jaroso, Spain, all contained impurities that complicate interpretation of the experiments. An impure sample from Golconda, Nevada had a small endothermic peak below 400 °C, which was attributed to goethite. Two reportedly inhomogeneous jarosites from Darwin, California exhibited a moderate endotherm between 100 and 200 °C. Differential thermal analysis of alunite-jarosite solid solutions and mixtures reported by Alias and Girella (1965, 1968) exhibit strong endotherms at $T > 400$ °C. Jambor (1999) noted that although the complete alunite-jarosite solid solution can be synthesized, intermediate compositions are rare in natural samples. Caillère and Hénin (1954) described the chemistry and thermal behavior of an aluminous jarosite from Djebel Debar, Algeria. Differential thermal and thermogravimetric analysis showed the jarosite lost water (11.5 wt.%) at about 450 °C; a similar curve was reported for jarosite from Saint Felix de Palliers, France. Many of the thermal patterns for natural jarosites reported in the literature include subtle complexities at lower temperatures (<400 °C) that may reflect sample impurities, excess water, or an hydronium ion component. For example, the natural hydronium jarosite from Silesia studied by Kubisz (1961) contained a significant clay component. Thermal analysis of a sample of hydronium jarosite mixed with minor amounts of alunite, quartz, and kaolinite from weathered schist from Iza Cave, Romania lost 5.79% of its mass on heating to 163 °C attributed to H_3O followed by higher-temperature losses of 9.75% attributed to decomposition of OH (Tamas and Ghergari, 2003).

Our study shows that near end-member samples of natural stoichiometric jarosite and natrojarosite exhibit relatively simple thermal behavior patterns. Water is evolved in a single thermal event between 400 and 500 °C. Low-temperature (<400 °C) endothermic reactions that appear to be characteristic of synthetic jarosites, synthetic natrojarosites, hydronium jarosites, and impure samples were not observed in the Pena Blanca and Cyprus samples. The single water loss in the pure natural samples occurs at slightly higher temperatures for jarosite relative to natrojarosite. Simultaneous evolved gas analysis for the Pena Blanca jarosite indicates that a small amount of SO_2 evolved in a reaction that overlapped water loss.

3.5. Spectroscopy

Spectroscopy is a useful tool for providing complimentary information on the composition and atomic structure of the jarosite group of minerals. In the near- and mid-infrared spectral region (~2 to 25 μm), transmission measurements can reveal the presence of vibrational absorptions of molecular bonds. Jarosite infrared spectroscopy is sensitive to vibrational modes of OH^-, H_2O, H_3O^+, SO_4^{2-}, and Fe–O bonds (Adler and Kerr, 1965; Kubisz, 1972; Serna et al., 1986; Drouet and Navrotsky, 2003; Bishop and Murad, 2005; Swayze et al., 2008). Fig. 7 shows the infrared-active fundamental absorptions of the jarosite-group minerals for which many vibrational absorptions are detectable. The relatively narrow hydroxyl stretch absorption (ν_{OH}) is located near 2.95 μm, the ν_3 stretch doublet of SO_4^{2-} is centered near 8.7 μm, the Fe–O–H in-plane-bend (δ_{OH}) is positioned near 9.9 μm, and the narrow shoulder on the long wavelength side of the δ_{OH} bend is the ν_1 stretch of SO_4^{2-} (Serna et al., 1986). There is some uncertainty regarding the assignment of absorptions at 15.0 μm to the ν_4 stretch of SO_4^{2-} and at 22.3 μm to the ν_2 stretch of SO_4^{2-} as these absorptions may be due to Fe–O related vibrations similar to the ν_{Fe-O} doublet absorption centered near 20 μm (Breitinger et al., 1997). The weak absorption near 17.1 μm belongs to the out-of-plane Fe–O–H bend (γ_{OH}) based on observations of a deuterated synthetic jarosite (Serna et al., 1986), whereas the less intense absorption near 6 μm is due to the H–O–H bend in water (δ_{H2O}) (Bishop and Murad, 2005).

There is spectral evidence for coexisting jarosite and natrojarosite phases in some of the natural samples. Fig. 8 shows details of a cluster of continuum-removed absorptions located near 5 μm in spectra of natural and synthetic jarosites. A spectral continuum is the local spectral slope projected over the top of an absorption band.

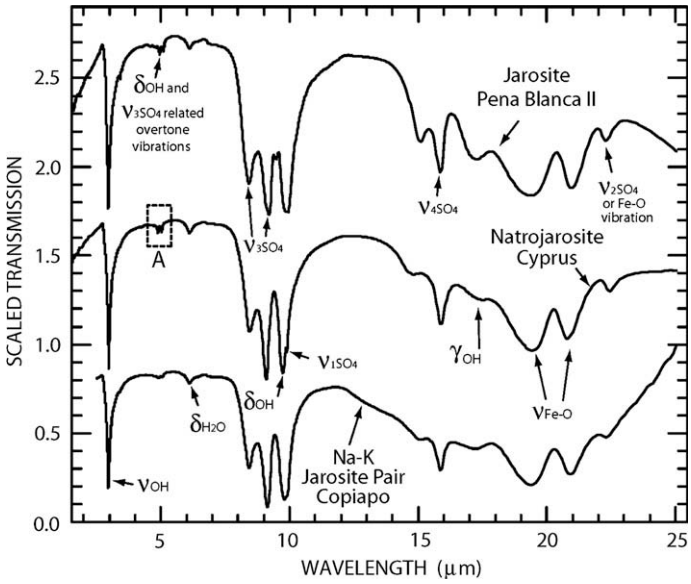

Fig. 7. Transmission spectra of end-member jarosite and natrojarosite and a natural mixture of these two end-members. Vibrational assignments are based on those given in Serna et al. (1986), Breitinger et al. (1997), and Bishop and Murad (2005). Dashed box (A) encompasses an absorption complex attributed to OH^- and SO_4^{-2} related absorptions shown in more detail in Fig. 8. Spectra are offset vertically to eliminate overlap.

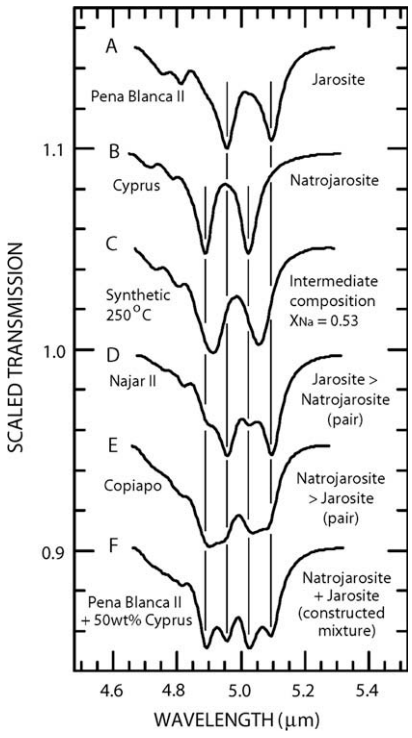

Fig. 8. Transmission spectra of natural end-members jarosite and natrojarosite (A–B), a synthetic intermediate-composition jarosite (C), and natural jarosite pairs (D–E). Spectrum F is a constructed mixture of 50 wt.% jarosite (A) and natrojarosite (B). Vertical lines mark wavelength positions of absorptions with end-member compositions. Spectra are offset vertically and continuum removed for clarity. X_{Na} refers to the mole fraction of Na in the synthetic jarosite sample as measured by atomic absorption spectroscopy (see Stoffregen, 1993, Table 3).

A continuum can be removed by fitting a straight line to the uppermost margins of an absorption and then dividing the absorption reflectance values by this line, hence allowing absorptions with different continuum slopes to be easily compared (Clark and Roush, 1984). Comparison of spectra from deuterated and non-deuterated synthetic alunites indicates that absorptions in this spectral region can be assigned to the ν_{3SO4} stretch and δ_{OH} bend overtone absorptions (Breitinger et al., 1999). These same assignments have been suggested for similar absorptions in jarosite (Bishop and Murad, 2005). The doublet absorptions at 4.96 and 5.10 μm in jarosite (spectrum A) shift to 4.89 and 5.02 μm in natrojarosite (spectrum B), respectively, as a function of composition, thus allowing detection of multiple compositional jarosite phases within a sample. Apparently this is the clearest spectral region for determining the presence of multiple components or degree of solid solution, whether done in transmission or reflectance. As expected, the spectrum of an intermediate-composition high-temperature synthetic jarosite prepared by Stoffregen (see Stoffregen, 1993) has just two absorptions located at wavelengths intermediate between those of the end-member spectra (spectrum C) indicating true solid solution in the sample. Alternatively, the spectrum of sample Najar-II (spectrum D) has two sets of double absorptions closely matching the wavelength positions of the end-member spectra but of different strengths indicating that jarosite is more abundant than natrojarosite. Similarly, the spectrum of the Copiapo sample (spectrum E) has overlapping doublets (forming two broad square-bottomed absorptions) indicating two components of near-end-member composition but in nearly equal proportions. Spectrum F is a physical mixture of the end-member Pena Blanca II (K) and Cyprus (Na) samples in equal proportions. If samples D or E had

true intermediate solid-solution compositions, their spectra would consist of a single doublet with a wavelength position similar to that of spectrum C. Therefore, with infrared spectroscopy it may be possible to determine not only the composition and relative proportions of jarosite phases in a sample, but also the extent of solid solution within these phases using Gaussian or Voigt curve modeling and by making some assumptions about sample grain size (because grain size has an influence on detection limits).

3.6. Lack of Na–K solid solution in low-temperature samples

An issue of particular interest in this study is whether or not there is low-temperature ($\leqslant 100$ °C) solid solution between jarosite and natrojarosite. Observations of unit-cell dimensions for the 32 natural stoichiometric hydrothermal and supergene jarosites and natrojarosites examined in this study indicate that all of them are near-end-members of either jarosite or natrojarosite (Table 1, Fig. 1). Some samples consisted of a physical mixture of coexisting jarosite and natrojarosite end-member pairs. The unit-cell parameters of these jarosite and natrojarosite end members do not overlap (Table 2, Figs. 1 and 2), and we do not observe any cell dimensions intermediate between jarosite and natrojarosite end members, which would be diagnostic for solid solution between jarosite and natrojarosite. These findings are substantiated by thermogravimetric and reflectance-spectroscopy studies of the samples reported herein (Figs. 6 and 8). We conclude that there is no evidence for low-temperature solid solution between jarosite and natrojarosite in the 23 diverse samples we studied; this finding was also reported in Desborough et al. (2004, 2006).

Previously, it has been presumed that there is solid solution between jarosite and natrojarosite at all temperatures. For example, Brophy and Sheridan (1965) reported a continuous solid solution between the end members jarosite, natrojarosite, and hydronium jarosite under low-temperature and low-pressure conditions. Stoffregen (1993) and Stoffregen et al. (2000) suggested that "The nearly ideal behavior of jarosite and natrojarosite at 200° strongly suggests that there is complete miscibility on the jarosite-natrojarosite binary down to 25 °C". However, there was no direct evidence of jarosite-natrojarosite miscibility at low temperatures. Chemical analyses that show intermediate compositions between end-member K and Na in low-temperature samples likely represent analysis of a physical mixture of end-member pairs. As previously noted, low-temperature jarosite minerals are generally very fine-grained, which prohibits their separation for chemical analysis. Also, the grains generally are too small to resolve by electron-probe microanalysis.

Our observation of the lack of low-temperature jarosite–natrojarosite solid solution is consistent with the findings of Glynn (2000) and Papike et al. (2007). Glynn (2000, Fig. 3) used a Lippmann phase diagram of the jarosite–natrojarosite aqueous system at 25 °C to demonstrate that there is a high probability of the absence of solid solution at low temperature because of the large orders of magnitude of difference in the solubility products of the end members. Papike et al. (2007) found end-member jarosite and natrojarosite compositions in their electron microprobe study of eight hypogene and three supergene samples of jarosite and natrojarosite.

Another issue of importance in this study is the presence of hydronium-bearing jarosite in natural low-temperature samples. The presence of hydronium is usually inferred from low alkali content in the mineral because hydronium is difficult to directly measure (Stoffregen et al., 2000). We detected the possible presence of hydronium-bearing jarosite in only one natural stoichiometric sample that we studied (see sample 81196u in Figs. 5 and 6). This suggests that terrestrial hydronium-bearing jarosite likely is unstable over geologic timescales.

3.7. Evidence for a solvus in hydrothermal systems

Stoffregen et al. (2000) demonstrated higher-temperature (e.g., 140–200 °C) solid solution between jarosite and natrojarosite. Based on the near-end-member composition and cell dimensions observed for the 32 natural supergene and hydrothermal jarosites and natrojarosites in our study, we hypothesize that there is a solvus in the jarosite–natrojarosite system below about 140 °C (also see Desborough et al., 2004, 2006). For samples of adequate zoning size or grain size, quantitative electron-probe microanalysis data for several natural hydrothermal samples examined in this study show only end-member jarosite and natrojarosite compositions for individual grains or zones. Electron-probe microanalysis results of the hydrothermal samples also reveal that there are no significant deficiencies (vacancies) in the A, B, or X sites. This is consistent with the electron microprobe studies of Papike et al. (2007) who also found their microprobe results to be consistent with the proposal of a solvus (miscibility gap) in the jarosite–natrojarosite system by observing only near end-members of jarosite and natrojarosite when using a 1-μm electron beam in traversing zoned bands of jarosite–natrojarosite mixtures that are too small to resolve in both energy-dispersive SEM studies and WDS microprobe studies. Electron micrographs shown in Figs. 3 and 4, herein, are compelling evidence of the segregation of jarosite and natrojarosite in hydrothermal samples.

Prior EPMA studies of natural jarosite from Goldfield, Nevada and Syama, Mali by Vasconcelos et al. (1994, Table 3) used a sample current of 30 nA, accelerating voltage of 15 kV, and beam diameter of 3–5 μm for "supergene" jarosites; they report extensive solid solution of Na and K and cation deficiencies between 5 and 52 mol% in the monovalent site. Sample currents as high as 30 nA will result in K and/or Na migration during microprobe analysis of jarosites; this may lead to an apparent cation deficiency. Drouet and Navrotsky (2003, Table 1) analyzed synthetic jarosites with an electron microprobe and report up to 72 mol% alkali-site deficiency in K–H_3O jarosite. However, they do not state the analytical conditions for the electron microprobe analysis. Jamieson et al. (2005) report as much as 60 mol% H_30 in the alkali site of recently-formed jarosite from the Richmond mine, Iron Mountain, California based on energy-dispersive analysis using an electron probe (see section below).

Stoffregen (2006) states that "Increasing departures from ideality with decreasing temperature are not precluded by the experimental data, but a solvus in the system jarosite–natrojarosite is considered unlikely". However, we believe the findings of Glynn (2000), cited above, are strong evidence that a solvus can exist at some temperature below about 140 °C in order to produce the end-member jarosite–natrojarosite pairs that we have observed.

4. NON-STOICHIOMETRIC SUPERGENE JAROSITE MINERALS

Jamieson et al. (2005) report chemical data for non-stoichiometric jarosites that occur as stalactites in the abandoned Richmond mine at Iron Mountain, California where mining occurred between the 1860s and 1962. They analyzed jarosites using electron probe EDS and WDS methods and found that the Fe^{+3} octahedral site was Fe-deficient with an (Fe + Al):S range of 2.5–2.97:2, rather than 3:2 as required for stoichiometry. The molar sum of K + Na in the alkali site ranged from 0.46 to 0.88 and the balance was assumed to be hydronium. The size of intergrown K-rich and Na-rich grains determined by electron-probe imaging was so small that microprobe analysis using a focused electron beam could not resolve the composition of individual grains (Jamieson et al., 2005, Fig.7). Thus compositional data are for aggregates of K-rich and Na-rich grains. No data for cell parameters were given.

Fragments of the Richmond mine jarosite-bearing stalactites were provided for our study by Heather Jamieson. Some of these were used for XRD, spectral, and heating studies; others were mounted and polished for EPMA. Fragments used for XRD studies were ground in ethanol in a mechanical mortar and pestle and mixed with 10 wt.% alumina for the internal standard. Electron-probe microanalysis of 37 five-μm areas on three fragments gave (Fe + Al):S ratios of 2.63–2.97:S giving vacancy ratios of 1–12% for the octahedral Fe site; values of (Na + K):S ranged from 0.51 to 0.84. Spectral examination showed the presence of hydronium (Swayze et al., 2008); this was confirmed by heating at 240 °C for 24 h, which produced $Fe(OH)SO_4$ (Desborough et al., 2004, 2006) and an associated weight loss of 11.9 weight percent due to water vapor. Cell parameters were measured for 12 natural non-stoichiometric jarosites in five fragments and ranged from $a = 7.313$–7.330 Å, and $c = 17.010$–17.180 Å as shown on Fig. 9; the mean and σ values were $a = 7.319$, $\sigma = 0.005$ and $c = 17.112$, $\sigma = 0.051$. Fig. 9 shows that there is a slight overlap of c-values of three samples of the natural non-stoichiometric group and natural stoichiometric group; however, the corresponding a-values for those three samples show no overlap of the two groups. In a previous report the natural stoichiometric group was referred to as "mature", in contrast to the non-stoichiometric group which was called "modern" due to their young age (Desborough et al., 2006, Fig. 5). The term "non-stoichiometric" (for the "modern" samples) is used here because it is more descriptive. It also applies to most synthetic jarosites prepared at temperatures in the range of 90–100 °C (Kubisz, 1970; Drouet and Navrotsky, 2003).

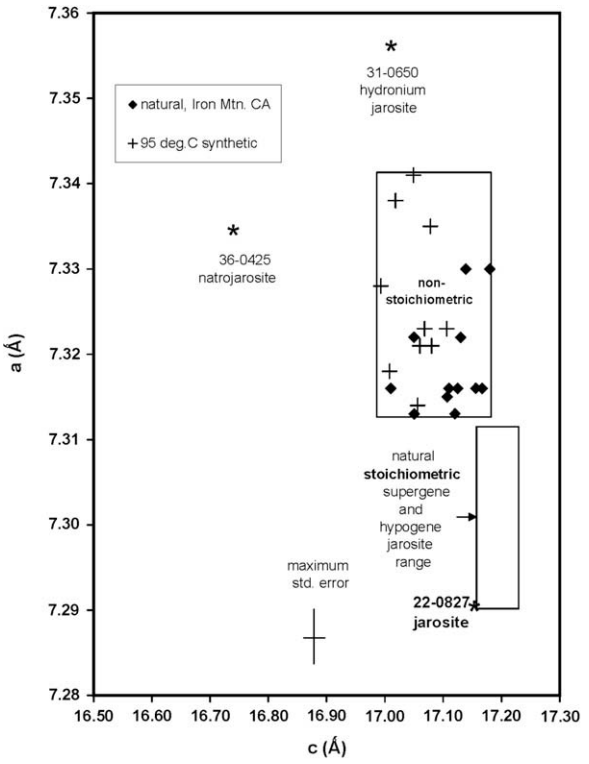

Fig. 9. Range of a- and c-cell parameters for natural (Iron Mtn., California) non-stoichiometric supergene jarosites, non-stoichiometric 95 °C synthetic jarosites (see Desborough et al., 2006), and natural stoichiometric supergene and hypogene jarosites (this study). Jarosite-family end members from the International Center for Diffraction Data (ICDD) Powder Diffraction File also are shown.

A natural non-stoichiometric jarosite from mine waste in the Rio Tinto mining district near Huelva, Spain (sample 7–11–3–8) recently was reported by Basciano and Peterson (2007). This sample had 9 mol% Fe deficiency, and the alkali site had 85 mol% K + Na. Basciano and Peterson (2007, 2008) provide plots of both synthetic and natural jarosite, natrojarosite, and hydronium–jarosite samples.

5. SUMMARY AND CONCLUSIONS

The natural stoichiometric jarosite and natrojarosite samples from diverse environments analyzed in this study have a very narrow range in a and c unit-cell dimensions, whether they are of hydrothermal or supergene origin. For the 32 natural stoichiometric jarosite and natrojarosite samples studied, there is no evidence of significant hydronium substitution (>5 mol%) in the monovalent or alkali site. A possible exception to the previous statement is supergene sample 81196u, which may have a small amount of either hydronium jarosite or alkali-site cation deficiency based on electron microprobe and TGA analyses. Quantitative electron-probe microanalyses of stoichiometric natural jarosite and natrojarosite of hydrothermal origin reveal no cation or anion deficiencies. These findings are in contrast to results for non-stoichiometric samples we examined, which exhibit vacancy ratios of 1–12% for the octahedral Fe site.

This indicates that hydronium jarosite likely is unstable in most terrestrial environments over geologic timescales, and that many jarosite and natrojarosite minerals found in nature do not, or no longer, contain deficiencies and, hence, are relatively stable. Therefore, stoichiometric jarosite minerals may make only a limited contribution to acid generation in many natural systems. However, transformation of non-stoichiometric jarosite to stoichiometric jarosite minerals may contribute to acid generation.

No evidence was found for significant solid solution (e.g., >5 mol%) of Na in jarosite or K in natrojarosite in the 23 natural samples examined in this study. Instead, four hydrothermal samples and five supergene samples consisted of pairs of both end-member jarosite and end-member natrojarosite. We also show spectral evidence for coexisting jarosite and natrojarosite phases in some of the natural samples.

Backscattered electron images of several polished thin sections of hydrothermal samples reveal textures of intergrown jarosite and natrojarosite end members that we interpret as forming from subsolidus or solid-state diffusion segregation at low temperature. There is good evidence in the literature for extensive solid solution between jarosite and natrojarosite at high(er) temperatures (e.g., ~200 °C); however, because we see only end-member jarosite and natrojarosite in our natural samples, we hypothesize that there is a solvus between 140 and 25–30 °C. Supergene samples containing end-member pairs of jarosite and natrojarosite are consistent with a lack of solid solution at lower temperatures (e.g., <30 °C).

ACKNOWLEDGMENTS

Charles Alpers, John Jambor (deceased), and Roger Stoffregen kindly reviewed an earlier version of this paper and we thank them for helpful critical comments and suggestions that we have incorporated. We also thank Jim Papike for his valuable suggestions. We are grateful to Roger Stoffregen for providing the synthetic high-temperature intermediate jarosite–natrojarosite used for the spectral illustration, and to Heather Jamieson for providing jarosite-bearing stalactites from the Richmond mine. Philip Goodell generously provided the high-purity natural Pena Blanca, Mexico sample. Funding for this work was provided by the U.S. Geological Survey Mineral Resources Program.

REFERENCES

Adler H. H. and Kerr P. F. (1965) Variations in infrared spectra, molecular symmetry and site symmetry of sulfate minerals. *Am. Mineral.* **50**, 132–147.

Akai J., Kawamoto K., Akai K., Nakano S. (1997) Biogenic contribution to the formation of iron ore in Gumma Iron Mine, central Japan. In: *Proc. 30th Int. Geol. Congr.* 9, pp. 199–208.

Alias L. J. and Girella V. F. (1965) A study by differential thermal analysis of the alunite–jarosite system. In *Proc. First Int. Thermal Analysis Conf.* Macmillan and Company, Ltd., pp. 224–225.

Alias L. J. and Girella V. F. (1968) Estudio por análisis térmico diferencial de soluciones sólidas y mezclas de jarosita y alunita. *Estud. Geol.* **24**, 79–83.

Alpers C. N. and Brimhall G. H. (1989) Paleohydrologic evolution and geochemical dynamics of cumulative supergene metal enrichment at La Escondida, Atacama Desert, northern Chile. *Econ. Geol.* **84**, 229–255.

Alpers C. N., Nordstrom D. K. and Ball J. W. (1989) Solubility of jarosite solid solutions precipitated from acid mine waters, Iron Mountain, California. *U.S.A. Sci. Geol. Bull.* **42**, 281–298.

Alpers C. N., Rye R. O., Nordstrom D. K., White L. D. and Bi-Shia K. (1992) Chemical, crystallographic and stable isotope properties of alunite and jarosite from acid-hypersaline Australian lakes. *Chem. Geol.* **96**, 203–226.

Alpers C. N., Blowes D. W., Nordstrom D. K. and Jambor J. L. (1994) Secondary minerals and acid mine-water chemistry. In *The Environmental Geochemistry of Sulfide Mine-Wastes* (eds. D. W. Blowes and J. L. Jambor). Mineral. Assn. Canada Short Course Handbook 22, pp. 247–270.

Basciano L. C. and Peterson R. C. (2007) Jarosite–hydronium jarosite solid-solution series with full iron site occupancy: mineralogy and crystal chemistry. *Am. Mineral.* **92**, 1464–1473.

Basciano L. C. and Peterson R. C. (2008) Crystal chemistry of the natrojarosite–jarosite and natrojarosite–hydronium jarosite solid-solution series: a synthetic study with full Fe site occupancy. *Am. Mineral.* **93**, 853–862.

Bish D. L. and Duffy C. J. (1990) Thermogravimetric analysis of minerals. In *Thermal Analysis in Clay Science* (eds. J. W. Stiki and D. L. Bish). Clay Min. Soc. Workshop Lectures 3, pp. 96–157.

Bishop J. L. and Murad E. (2005) The visible and infrared spectral properties of jarosite and alunite. *Am. Mineral.* **90**, 1100–1107.

Breitinger D. K., Krieglstein R., Bogner A., Schwab R. G., Pimpl Th. H., Mohr J. and Schukow H. (1997) Vibrational spectra of synthetic minerals of the alunite and crandallite type. *J. Mol. Struct.* **408**(409), 287–290.

Breitinger D. K., Schukow H., Belz H.-H., Mohr J. and Schwab R. G. (1999) Two-phonon excitations in IR and NIR spectra of alunites. *J. Mol. Struct.* **480**(481), 677–682.

Briggs P. H. and Meier A. L. (2002) The determination of forty-two elements in geological materials by inductively coupled plasma-mass spectrometry. *USGS Open-File Rept*. 02-223-I.

Brophy G. P. and Sheridan M. F. (1965) Sulfate studies, IV: the jarosite–natrojarosite–hydronium jarosite solid solution series. *Am. Mineral.* **50**, 1595–1607.

Burger P. V., Papike J. J., Shearer C. K. and Karner J. M. (2006) The role of fluid chemistry and crystallization kinetics in Na and K zoning in jarosite. *Lunar Planet. Inst. Workshop on Martian Sulfates*. #7019 (abstr.).

Butler B. S., Loughlin G. F. and Heikes V. C. (1920) The ore deposits of Utah. *USGS Prof. Pap*. 111.

Caillère S. and Hénin S. (1954) Sur quelques minéraux du Djebel Debar. *Bull. Soc. Fr. Miner. Crist.* **77**, 479–490.

Clark R. N. and Roush T. L. (1984) Reflectance spectroscopy: quantitative analysis techniques for remote sensing applications. *J. Geophys. Res.* **89**, 6329–6340.

Cravotta III C. A. (1994) Secondary iron-sulfate minerals as sources of sulfate and acidity In *Environmental Geochemistry of Sulfide Oxidation* (eds. C. N. Alpers and D. W. Blowes). Am. Chem. Soc. Symp. Series 550, pp. 345–364.

Desborough G. A., Leinz R., Smith K., Hageman P., Fey D. and Nash T. (1999) Acid generation and metal mobility and some metal-mining related wastes in Colorado. *USGS Open-File Rept*. 99–322.

Desborough G. A., Smith K. S., Swayze G. A., Diehl S. F., Lowers H. A., Hammarstrom J. M., Driscoll R. L. and Leinz R. W. (2004) A detailed comparison of natural and synthetic jarosite minerals. *Geol. Soc. Am. Abstr. Prog.* **36**(5), 337 (abstr.).

Desborough G. A., Smith K. S., Lowers H. A., Swayze G. A., Hammarstrom J. M., Diehl S. F., Driscoll R. L. and Leinz R. W. (2006) The use of synthetic jarosite as an analog for natural jarosite. In *Proceedings of the Seventh International Conference on Acid Rock Drainage*. St. Louis, Missouri, pp. 458–475.

Drouet C. and Navrotsky A. (2003) Synthesis, characterization, and thermochemistry of K–Na–H_3O jarosites. *Geochim. Cosmochim. Acta* **67**, 2063–2076.

Dutrizac J. E. and Jambor J. L. (2000) Jarosites and their application in hydrometallurgy. In *Sulfate Minerals, Crystallography, Geochemistry, and Environmental Significance* (eds. C. N. Alpers, J. L. Jambor and D. K. Nordstrom). Mineral. Soc. Am. Rev. Mineral. Geochem. 40, pp. 405–443.

Dutrizac J. E. and Kaiman S. (1976) Synthesis and properties of jarosite-type compounds. *Can. Mineral.* **14**, 151–158.

Gasharova B., Gottlicher J. and Becker U. (2005) Dissolution at the surface of jarosite – an in-situ AFM study. *Chem. Geol.* **215**, 499–516.

Glynn P. (2000) Solid-solution solubilities and thermodynamics: Sulfates, carbonates, and halides. In *Sulfate Minerals, Crystallography, Geochemistry, and Environmental Significance* (eds. C. N. Alpers, J. L. Jambor and D. K. Nordstrom). Mineral. Soc. Am. Rev. Mineral. Geochem. 40, pp. 481–511.

Ivarson K. C. (1973) Microbiological formation of basic ferric sulfates. *Can. J. Soil Sci.* **53**, 315–323.

Ivarson K. C., Ross G. J. and Miles N. M. (1982) Microbiological transformations of iron and sulfur and their applications to acid sulfate soils and tidal marshes. In *Acid Sulfate Weathering* (eds. J. A. Kittrick, D. S. Fanning and I. R. Hossner). SSSA Spec. Pub. 10, pp. 57–76.

Jambor J. L. (1999) Nomenclature of the alunite supergroup. *Can. Mineral.* **37**, 1323–1341.

Jambor J. L., Nordstrom D. K. and Alpers C. N (2000) Metal–sulfate salts from sulfide mineral oxidation. In *Sulfate Minerals, Crystallography, Geochemistry, and Environmental Significance* (eds. C. N. Alpers, J. L. Jambor and D. K. Nordstrom). Mineral. Soc. Am. Rev. Mineral. Geochem. 40, pp. 303–350.

Jamieson H. E., Robinson C., Alpers C. N., Nordstrom D. K., Poustovetov A. and Lowers H. A. (2005) The composition of coexisting jarosite-group minerals and water from the Richmond mine, Iron Mountain, California. *Can. Mineral.* **43**, 1225–1242.

Kato T. and Miúra Y. (1977) The crystal structures of jarosite and svanbergite. *Mineral. J.* **8**, 419–430.

Klingelhöfer G., Morris R. V., Bernhardt B., Schroder C., Rodionov D., a Jr P. A., Yen A., Gellert R., Evlanov E. N., Zubkov B., Foh J., Bonnes U., Kankeleit E., Gutlich P., Ming D. W., Renz F., Wdowiak T., Squyres S. W. and Arvidson R. E. (2004) Jarosite and hematite at Meridiani planum from Opportunity's Mossbauer spectrometer. *Science* **306**, 1740–1745.

Kubisz J. (1961) Natural hydronium jarosites. *Bull. Acad. Polon. Sci. Ser. Sci. Geol. Geog.* **9**, 195–200.

Kubisz J. (1970) Studies on synthetic alkali-hydronium jarosites. I. Synthesis of jarosite and natrojarosite. *Mineral. Polonica* **1**, 47–57.

Kubisz J. (1971) Studies on synthetic alkali-hydronium jarosites. II. Thermal investigations. *Mineral. Polonica* **2**, 51–59.

Kubisz J. (1972) Studies on synthetic alkali-hydronium jarosites. III. Infrared absorption study. *Mineral. Polonica* **3**, 23–35.

Kulp J. L. and Adler H. H. (1950) Thermal study of jarosite. *Am. J. Sci.* **8**, 275–287.

Lapakko K. and Berndt M. (2003) Comparison of acid production from pyrite and jarosite. In *Proceedings of the Sixth International Conference on Acid Rock Drainage*. Cairns, QLD, Australia, 7p.

Lueth V. W., Rye R. O. and Peters L. (2005) "Sour Gas" hydrothermal jarosite: ancient to modern acid–sulfate mineralization in the southern Rio Grande Rift. *Chem. Geol.* **215**, 339–360.

Martinez-Frias J., Lunar R., Rodriguez-Losada J. A., Delgado A. and Rull F. (2004) The volcanism-related multistage hydrothermal system of El Jaroso (SE Spain): implications for the exploration of Mars. *Earth Planet. Space* **56**, 5–8.

Milliken R. E., Swayze G. A., Arvidson R. E., Bishop J. L., Clark R. N., Ehlmann B. L., Green R. O., Grotzinger J. P., Morris R. V., Murchie S. L., Mustard J. F. and Weitz C. (2008) Opaline silica in young deposits on Mars. *Geology* **36**, 847–850.

Mitchell R. S. and Giannini W. F. (1958) Natrojarosite from near the Montana–Wyoming line. *Am. Mineral.* **43**, 1205–1210.

Nordstrom D. K. and Alpers C. N. (1999) Geochemistry of acid mine waters. In *The Environmental Geochemistry of Mineral Deposits* (eds. G. S. Plumlee and M. J. Logsdon). Soc. Econ. Geol. Rev. Econ. Geol. 6A, pp. 133–160.

Paktunc D. and Dutrizac J. E. (2004) Characterization of arsenate-for-sulfate substitution in synthetic jarosite using x-ray diffraction and x-ray absorption spectroscopy. *Can. Mineral.* **41**, 905–919.

Papike J. J., Karner J. M., Spilde M. N. and Shearer C. K. (2006) Terrestrial analogs of martian sulfates: Major and minor systematics of alunite–jarosite from Goldfield, Nevada. *Am. Mineral.* **91**, 1197–1200.

Papike J. J., Burger P. V., Karner J. M., Shearer C. K. and Lueth V. W. (2007) Terrestrial analogs of martian jarosites: major, minor element systematics and Na–K zoning in selected samples. *Am. Mineral.* **90**, 444–447.

Polyak V. J. and Provencio P. (2001) By-product materials related to H_2S–H_2SO_4 influenced speleogenesis of Carlsbad, Lechuguilla, and other caves of the Guadalupe Mountains, New Mexico. *J. Cave Karst Stud.* **63**, 23–32.

Rodriguez N., Menendez N., Tornero J., Amils R. and de la Fuente V. (2005) Internal iron biomineralization in *Imperata cylindrical*, a perennial grass: chemical composition, speciation and plant localization. *New Phytol.* **165**, 781–789.

Ross G. J., Ivarson K. C. and Miles N. M. (1982) Microbial formation of basic ferric sulfate systems and in soils. In *Acid Sulfate Weathering* (eds. J. A. Kittrick, D. S. Fanning and I. R. Hossner). SSSA Spec. Pub. 10, pp. 77–94.

Rye R. O. and Alpers C. N. (1997) The stable isotope geochemistry of jarosite. *USGS Open-File Rept.*, 97–88.

Serna C. J., Cortina C. P. and Garcia Ramos J. V. (1986) Infrared and Raman study of alunite–jarosite compounds. *Spectrochim. Acta* **42A**(6), 729–734.

Seyer S., Chen T. T. and Dutrizac J. E. (2001) Jarofix: addressing iron disposal in the zinc industry. *JOM* **53**, 32.

Smith A. M. L., Hudson-Edwards K. A., Dubbin W. E. and Wright K. (2006) Dissolution of jarosite $[KFe_3(SO_4)_2(OH)_6]$ at pH 2 and 8: insights from batch experiments and computational modelling. *Geochim. Cosmochim. Acta* **70**, 608–621.

Stoffregen R. (1993) Stability relations of jarosite and natrojarosite at 150–250 °C. *Geochim. Cosmochim. Acta* **57**, 2417–2429.

Stoffregen R. E. (2006) Experimental studies of jarosite and alunite at hydrothermal conditions. *Lunar Planet. Inst. Workshop on Martian Sulfates.* #7011 (abstr.).

Stoffregen R. E., Alpers C. N. and Jambor J. L. (2000) Alunite–jarosite crystallography, thermodynamics, and geochronology. In *Sulfate Minerals, Crystallography, Geochemistry, and Environmental Significance* (eds. C. N. Alpers, J. L. Jambor and D. K. Nordstrom). Mineral. Soc. Am. Rev. Mineral. Geochem. 40, pp. 453–479.

Swayze G. A., Smith K. S., Clark R. N., Sutley S. J., Pearson R. N., Rust G. S., Vance J. S., Hageman P. L., Briggs P. H., Meier A. L., Singleton M. J. and Roth S. (2000) Using imaging spectroscopy to map acidic mine waste. *Environ. Sci. Technol.* **34**, 47–54.

Swayze G. A., Desborough G. A., Smith K. S., Lowers H. A., Hammarstrom J. M., Diehl S. F., Leinz R. W. and Driscoll R. L. (2008) Understanding jarosite – from mine waste to Mars. In

Understanding Contaminants Associated with Mineral Deposits (ed. P. L. Verplanck). USGS Circular 1328, pp. 8–13.

Tamas T. and Ghergari L. (2003) Hydronium jarosite from Iza Cave (Rhodnei Mts., Romania). *Acta Mineral.-Petrog.*, Abstr. Ser. 1, Szeged, 102.

USDA (1975) Soil taxonomy: a basic system of soil classification for making and interpreting soil surveys (Natural Resources Conservation Service). *USDA Agr. Hbk.* **436**, 754.

Van Breemen N. (1982) Genesis, morphology and classification of acid sulfate soils in coastal plains. In *Acid Sulfate Weathering* (eds. J. A. Kittrick, D. S. Fanning and I. R. Hossner). SSSA Spec. Pub. 10, pp. 95–108.

Vasconcelos P. M., Brimhall G. H., Becker T. A. and Renne P. R. (1994) $^{40}Ar/^{39}Ar$ analysis of supergene jarosite and alunite: Implications to the paleoweathering history of the western USA and West Africa. *Geochim. Cosmochim. Acta* **58**, 401–420.

Wagner D. P., Fanning D. S., Foss J. E., Patterson M. S. and Snow P. A. (1982) Morphological and mineralogical features related to sulfide oxidation under natural and disturbed land surfaces in Maryland. In *Acid Sulfate Weathering* (eds. J. A. Kittrick, D. S. Fanning and I. R. Hossner). SSSA Spec. Pub. 10, pp. 109–126.

Warshaw C. M. (1956) The occurrence of jarosite in underclays. *Am. Mineral.* **41**, 288–296.

Welch S. A., Kirste D., Christy A. G., Beavis F. R. and Beavis S. G. (2008) Jarosite dissolution II – reaction kinetics, stoichiometry and acid flux. *Chem. Geol.* **254**, 73–86.

Associate editor: Tom McCollom